

---

This is an electronic reprint of the original article.  
This reprint may differ from the original in pagination and typographic detail.

Xie, Boxuan; Kerminen, Juho; Lietzen, Jari; Mela, Lauri; Ruttik, Kalle; Karakoc, Alp; Jäntti, Riku

## Flexible Thin Film Multi-antenna Integrated Backscatter Device

*Published in:*  
2024 IEEE Wireless Communications and Networking Conference, WCNC 2024 - Proceedings

*DOI:*  
[10.1109/WCNC57260.2024.10571338](https://doi.org/10.1109/WCNC57260.2024.10571338)

Published: 01/01/2024

*Document Version*  
Peer-reviewed accepted author manuscript, also known as Final accepted manuscript or Post-print

*Published under the following license:*  
CC BY

*Please cite the original version:*  
Xie, B., Kerminen, J., Lietzen, J., Mela, L., Ruttik, K., Karakoc, A., & Jäntti, R. (2024). Flexible Thin Film Multi-antenna Integrated Backscatter Device. In *2024 IEEE Wireless Communications and Networking Conference, WCNC 2024 - Proceedings* (IEEE Wireless Communications and Networking Conference). IEEE.  
<https://doi.org/10.1109/WCNC57260.2024.10571338>

---

This material is protected by copyright and other intellectual property rights, and duplication or sale of all or part of any of the repository collections is not permitted, except that material may be duplicated by you for your research use or educational purposes in electronic or print form. You must obtain permission for any other use. Electronic or print copies may not be offered, whether for sale or otherwise to anyone who is not an authorised user.

# Flexible Thin Film Multi-antenna Integrated Backscatter Device

Boxuan Xie, Juho Kerminen, Jari Lietzén, Lauri Mela, Kalle Ruttik, Alp Karakoç, Riku Jäntti  
Department of Information and Communications Engineering, Aalto University, 02150 Espoo, Finland  
Email: {firstname.lastname}@aalto.fi

**Abstract**—In the ambient backscatter communication (AmBC) system, a backscatter device (BD) transmits its messages to receivers by modulating and reflecting incident radio frequency (RF) signals from ambient RF emitters. Most existing studies investigate single-antenna BDs and fabricate them using the conventional printed circuit board (PCB) method. In this paper, we propose flexible inkjet-printed integrated backscatter devices (IBDs) for indoor backscatter radios. We investigate and fabricate both single-antenna and multi-antenna IBDs using the inkjet printing technique. Since the commonly used substrate polyethylene terephthalate (PET) for inkjet-printed electronics has highly lossy properties, the printed feeding lines in the RF become inefficient. We propose to overcome this problem by positioning the backscatter switch next to each antenna and controlling them simultaneously with the baseband backscatter signal. Attenuation of the baseband control signal in printed lines is low leading to increase in overall efficiency of the proposed system. We validate the prototypes with received backscatter signal strength measurements in an anechoic chamber. The result shows that the printed four-antenna IBD can benefit approximately 9 dB diversity gain compared with the single-antenna version.

**Index Terms**—Multi-antenna backscatter device, inkjet-printing, ambient backscatter communication, intelligent reflecting surface.

## I. INTRODUCTION

Ambient backscatter communication (AmBC) is a promising communication technology for low-energy ambient Internet of Things (IoT) applications in the beyond 5G (B5G) era [1], [2]. The AmBC enables backscatter devices (BDs) to harness the existing ambient radio frequency (RF) signals in the environment to communicate with low-power consumption, eliminating the need for active carrier signal generation [3]. In recent years, the AmBC has been viewed as a cornerstone of the future ultra-low-power machine type communications (MTC), offering unique solutions to various IoT applications [4], [5]. Furthermore, the AmBC system can also collaborate with the advent of reconfigurable intelligent surfaces (RIS), providing another dimension for enhancing the performance of IoT networks [6].

The major components of AmBC systems are the BDs and the reader. The BDs are responsible for modulating and reflecting the incident RF signals from ambient RF sources. The use of multiple antennas on both BDs and readers is investigated to enhance system performance. The AmBC scheme consisting of multiple ambient RF sources, the multi-antenna BD, and the multi-antenna reader is investigated in [7], [8]. The design and detection of backscatter signals in

AmBC systems, particularly in multi-antenna BDs, have been explored in [9], [10]. These works discussed that the diversity gains from multi-antenna BDs can benefit the signal-to-noise ratio (SNR) and bit error rate (BER) of the backscatter signal, thus improving the communication system performance. The use of multiple antennas can increase the coverage area and enhance the system's energy efficiency as demonstrated in drone-assisted AmBC IoT sensor networks [11]. Furthermore, in the cognitive AmBC system, multiple antennas can be leveraged to improve the performance even under uncertain ambient conditions [12].

As the vital hardware component of such AmBC systems, the BD designs have been widely investigated in the past decade. The need to produce low-cost BD nodes has raised interest in using inkjet-printed electronics, e.g., antennas and circuits [13]. In this respect, [14] demonstrated that inkjet printing could be utilized to create patch antenna arrays on flexible substrates. Furthermore, [15] examined the performance of thin film coplanar patch antennas attached to various background materials, highlighting the potential of inkjet-printed antennas for wireless communications at 2.4 GHz industrial, scientific, and medical (ISM) band. Interestingly, the use of printed antennas and circuits for making the BD is investigated in the realm of short-range mmWave backscatter communication at gigabit data rates [16], further demonstrating the potential of inkjet-printed backscatter devices.

Regarding hardware and practical system implementation, most of promising low-energy and low-data rate AmBC systems for indoor and outdoor backscatter radios prefer working at the sub-6 GHz frequency band. To the authors' best knowledge, the flexible and low-complexity inkjet-printed BD working at lower frequency bands has rarely been investigated in the literature. To explore this area, in this paper, we propose thin film inkjet-printed integrated backscatter devices (IBDs) for the AmBC at the 2.4 GHz ISM band. The IBDs integrate antennas and circuits on flexible thin film substrates for realizing the essential BD functionalities such as ambient signal harvest, modulation, and reflection.

We investigate and fabricate both single- and multi-antenna IBDs with low complexity using the inkjet printing technique. Each IBD consists of only a coplanar patch antenna, a positive-intrinsic-negative (PIN) diode, and a surface-mount device (SMD) control signal bias resistor. A BD node sends information by changing the termination of the antenna. Switching between loads is achieved by using the PIN diode with a

baseband control signal. The diode either shorts or opens the antenna terminals, offering two reflection coefficients  $\Gamma_1$  and  $\Gamma_2$ , resulting in  $\Gamma_1 = -\Gamma_2 = 1$ . The baseband control signal comes from either a microcontroller unit (MCU) or a function generator. We implement frequency shift keying (FSK) baseband signal for separating the direct path component (from the ambient RF source to reader) from the backscatter path component (from the BD to reader) in the frequency domain. The use of highly lossy PET substrates for inkjet-printed RF circuitry results in a dissipation of a significant amount of the fed power. This makes multiple antennas with printed feeding lines inefficient. In order to overcome this drawback, we propose to position backscatter switches next to each antenna. The switches are connected to the MCU over printed lines where the baseband control signal is fed through. Nevertheless, since the control signal operates at low frequencies, it does not attenuate as significantly as the RF signal.

We also compare the proposed IBD design with the conventional BD, for which the antenna is fed over coaxial cable [17]. In this paper, we address the conventional device as discrete backscatter device (DBD).

This work makes the following contributions:

- We propose and fabricate flexible and low-complexity inkjet-printed IBDs for the AmBC at 2.4 GHz ISM band. We also characterize the radiation pattern of the integrated coplanar patch antenna and antenna arrays;
- We investigate the IBDs under two AmBC configurations with well-known radio propagation models [18], i.e., bistatic dislocated and collocated schemes;
- We validate the IBD prototypes with over-the-air (OTA) measurements and simulations, and evaluate the results from two aspects: i). multi-antenna diversity gain at the IBDs; ii). backscattering performance of IBDs and DBDs from the received signal power aspect.

The rest of the paper is organized as follows. In Section II, the design and fabrication process of the IBDs are discussed and demonstrated. The proposed IBD prototypes are validated by experiments and simulations, and are compared with the DBDs in Section III. In Section IV, the measurement and simulation results are discussed and evaluated. Finally in Section V, conclusions are drawn and future work is discussed.

## II. DESIGN AND FABRICATION

In this section, the design and fabrication of the IBDs are introduced. As key components of the IBDs, the coplanar patch antenna and antenna array are introduced at first. Then, the principle, design, and fabrication of the IBDs are discussed.

### A. Antenna design and fabrication

As key components of the IBDs, the integrated coplanar patch antennas affect the IBDs' performance significantly. Hence, we first design and characterize the single antenna and antenna array without modulator circuitry. Such procedure ensures that the radiation capability of the antennas can enable ambient signal harvest and backscatter signal radiation at the aimed frequency band, before integrating them into the IBDs.

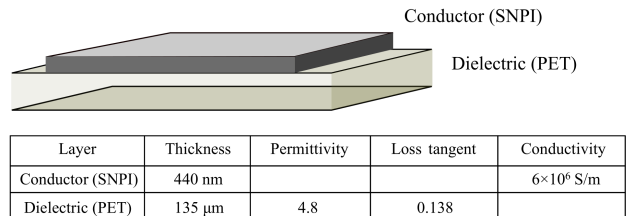
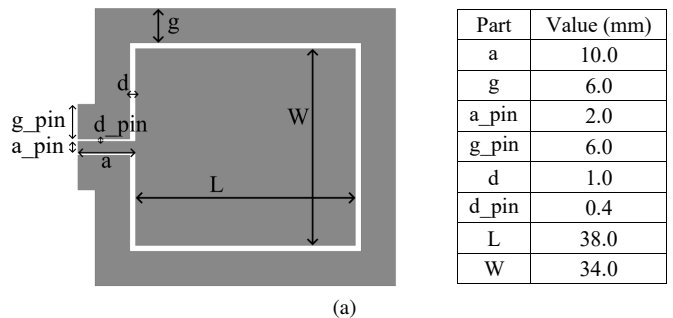


Fig. 1: Antenna design: (a) geometric parameters, (b) constituent material characteristics.

All antenna elements are designed to function at 2.45 GHz center frequency with a 10 dB bandwidth exceeding 100 MHz. The details of the inkjet-printed antenna designs can be found in [15]. Furthermore, dimensions of the prior antenna design are further optimized for improving the antenna performance and consuming less ink, thus resulting in more economic printing. This optimization process is conducted by design iteration with simulations in the Momentum Microwave solver of Keysight Advanced Design System (ADS) 2022. The final design shown in Fig. 1a is fabricated by inkjet-printing and then validated by carrying out antenna parameter measurements, where the utilized materials and their parameters are shown in Fig. 1b. Moreover, based on the single antenna design, a linear four-element antenna array with half-wavelength ( $\lambda/2$ ) separation is also designed to achieve higher directivity and gain than the single antenna.

The fabrication process of the antennas is introduced as follows. Mitsubishi NBSIJ-MU01 silver nanoparticle ink (SNPI) [19] is printed on top of NB-TP-3GU100 PET [19] substrate coated with microporous material ( $Al_2O_3$ -PVA) to form the conductive traces of the antenna. A low-cost inkjet printer EPSON WF-2840DWF is utilized for printing. Finally, 1500-watt photonic curing is applied on the printed sheet for 15 seconds to further sinter the conductive layer.

### B. Integrated backscatter devices design and fabrication

Designs of single-antenna IBD, shown in Fig. 2 and multi-antenna IBD, shown in Fig. 3 comprise the printed antenna elements and modulator circuitry. The modulator implementation utilizes a PIN diode SMP1345-079LF [20] connected to the antenna, switching the termination of the antenna between two loads  $Z_i \in \{Z_1, Z_2\}$ . Assuming the antenna is matched

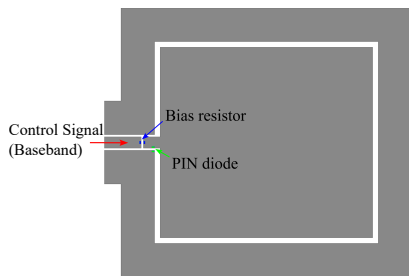


Fig. 2: Schematic of single-antenna IBD.

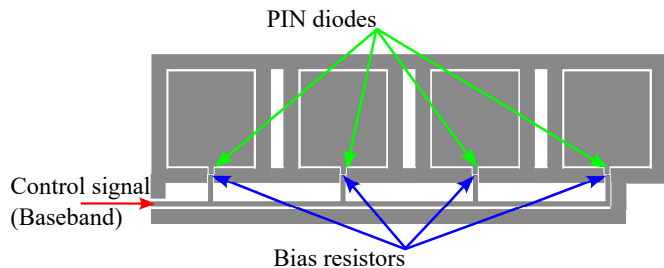


Fig. 3: Schematic of multi-antenna IBD.

to characteristic impedance  $Z_a$ , the complex reflection coefficient [18] is expressed by

$$\Gamma_i = \frac{Z_i - Z_a^*}{Z_i + Z_a}, \quad (1)$$

where  $*$  denotes the complex conjugation. The corresponding modulation factor  $M$  [18] is then

$$M = \frac{1}{4} |\Gamma_1 - \Gamma_2|^2. \quad (2)$$

When  $Z_1 = \infty$  and  $Z_2 = 0$  ideally resulting in  $\Gamma_1 = -\Gamma_2 = 1$ , the modulator achieves the maximum of  $M = 1$ , corresponding to the switch either open or short the antenna termination [18]. The switch control signal, a.k.a. baseband backscatter signal can be generated from either an MCU or a function generator, where the binary frequency shift keying (2FSK) is implemented in this research, such that the switching speed varies between predefined frequencies  $f_{m1}$  and  $f_{m2}$ . In addition, a 1.0 k $\Omega$  SMD resistor is applied between baseband feeding and the diode for biasing the control signal. When the ambient signal with a frequency of  $f_c$  illuminates the antenna, it gets mixed with control signals by switching operation. The modulated backscatter signals with frequencies  $f_c \pm f_{m1}$  and  $f_c \pm f_{m2}$  will reflect and deliver the data to the reader. The reader then detects and demodulates the backscatter signal to recover their carried information. However, the backscatter signals detection and recovery are usually difficult due to their low SNR, especially when the ambient signals cause direct path interference. Therefore, we develop the multi-antenna IBD with diversity gain that can directly improve the SNR or received backscatter signal power.

In order to achieve the antenna diversity gain, conventional PCB antenna design can refer to the well-known antenna array theory and design the microwave transmission lines and power

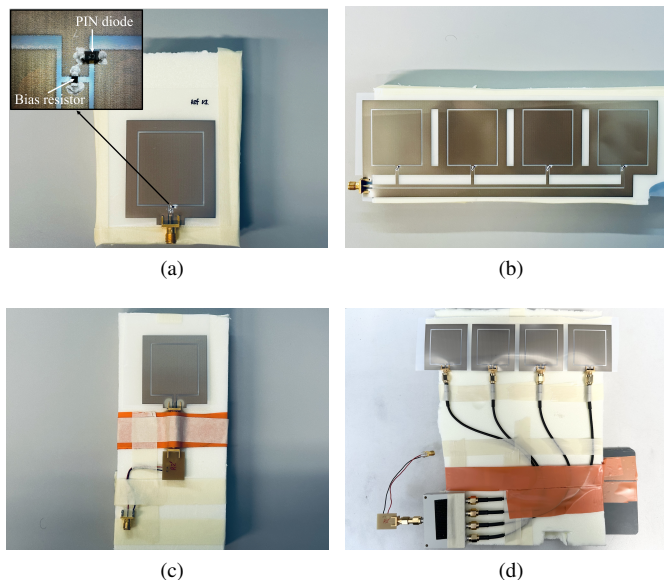


Fig. 4: Device prototypes: (a) single-antenna IBD, (b) multi-antenna IBD, (c) single-antenna DBD, (d) multi-antenna DBD.

splitters at the RF. However, these tasks become challenging for the inkjet-printed coplanar patch antenna and circuitry due to its lossy substrate and coplanar ground features. Instead, we design the power splitter at the baseband for splitting the control signal which modulates the incident ambient RF signal at all elements simultaneously. The multi-antenna IBD has four identical linearly-placed elements resembling the single-antenna IBD, with a half-wavelength ( $\lambda/2$ ) separation. The baseband power splitter splits the input control signal and feeds all elements. With the parallel baseband feeding, the diode of each element obtains approximately equal level control signal which then gets mixed with the incidence ambient signal. For simplicity, we assume that the incident ambient signal is a plane wave. Finally, we expect that the radiation of backscatter signal at the multi-antenna IBD resembles the radiation of a uniform linear array (ULA) with higher gain and directivity, compared with the single-antenna IBD.

Apart from printing and curing the schematics with the same method of fabricating the antennas, the fabrication process of the IBDs is completed with two more steps. The PIN diode and bias resistor are mounted to the schematic by using MG Chemicals conductive epoxy adhesive 9410. Finally, an oven is required for curing the adhesive. The completed single- and multi-antenna IBD are shown in Fig. 4a and 4b, respectively.

### III. EXPERIMENTS AND SIMULATIONS

#### A. Printed antenna and antenna array characterization

To verify the simulated and fabricated antenna design, both printed single antenna and antenna array are measured. They are characterized in terms of both return loss and far-field radiation pattern to analyze impedance matching and antenna parameters, such as realized gain and beamwidth. The return

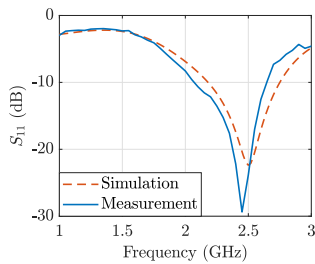


Fig. 5: Return loss simulation and measurement of the antenna.

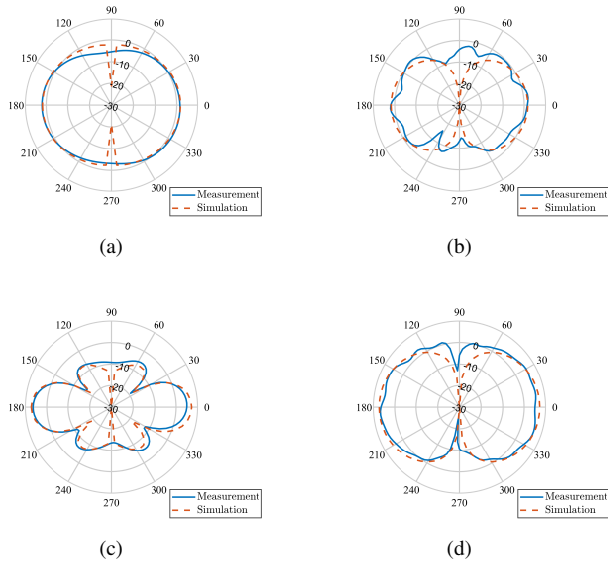


Fig. 6: Radiation pattern of the single antenna and antenna array at 2.4 GHz (Unit: dBi) : (a) azimuth cut of single antenna, (b) elevation cut of single antenna, (c) azimuth cut of antenna array, (d) elevation cut of antenna array.

loss of the single antenna design is measured with a Rohde & Schwarz vector network analyzer (VNA) ZNB 8, where microwave-absorbing foam panels are positioned around the antenna under test to eliminate noise. The radiation patterns of both single antenna and array are measured with StarLab antenna measurement system [21].

The measurement results are compared with simulations in terms of return loss ( $S_{11}$ ) shown in Fig. 5, and radiation patterns shown in Fig. 6. For the  $S_{11}$ , the fabricated single antenna is measured to have a dip of  $-29.36$  dB at 2.45 GHz with a 10 dB bandwidth of 575 MHz, where the simulation has a dip of  $-22.38$  dB at 2.50 GHz with a 10 dB bandwidth of 560 MHz. For the radiation pattern, the single antenna shows a simulated peak realized gain of 1.69 dBi and a measured peak gain of 1.89 dBi with a half power beamwidth (HPBW) around  $99^\circ$  at 2.42 GHz. The antenna array shows a simulated peak realized gain of 7.17 dBi and a measured peak gain of 6.34 dBi with an HPBW around  $33^\circ$ . The measured antenna parameters are in agreement with the simulations.



Fig. 7: OTA measurement setup: (a) bistatic collocated configuration, (b) bistatic dislocated configuration.

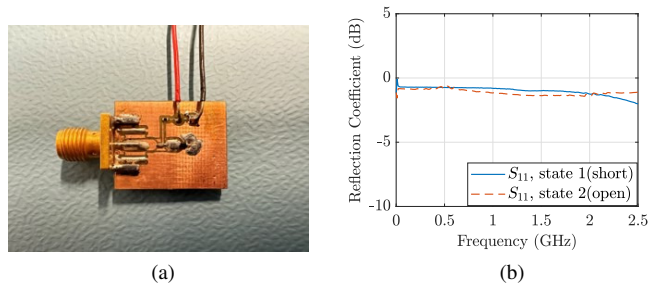


Fig. 8: Reflective backscatter tag: (a) PCB prototype, (b) reflection coefficients measurement.

### B. Over-the-air measurement and simulation

In this section, the fabricated single- and multi-antenna IBD are validated with the OTA backscatter radio measurement setups. In order to evaluate the performance of the proposed prototypes, the single- and multi-antenna DBD which have similar principles and schematics are also assembled as benchmarks for comparison. Moreover, the well-known backscatter radio propagation models [18] are implemented for simulating the received backscatter signal power of the scenarios under investigation. Therefore, the simulation environment is modeled with realistic parameters, which values approach our measurement setup.

For each measurement, the AmBC system is composed of an ambient RF source, a backscatter device under the test (DUT), and a receiver (RX) as a reader. At the ambient RF source, a directive flat patch antenna L-com HG2409P with 6.5 dBi gain and approximately  $70^\circ$  HPBW for both azimuth and elevation, is connected to a Rohde & Schwarz SMBV100A vector signal generator. The transmit power is set to 10 dBm, and the frequency of operation is 2.4 GHz. At the RX side, a real-time spectrum analyzer Siglent SSA3075X-R is connected to another directive flat patch antenna HG2409P, same as the transmit antenna. The received backscatter signal power is recorded by the spectrum analyzer and is then transferred to a laptop running MATLAB script for visualization.

The DUTs are shown in Fig. 4. Apart from the introduced single- and multi-antenna IBDs in Sec. II-B, the single- and multi-antenna DBDs which have similar principles and

schematics are also assembled as benchmarks for comparison. The single-antenna DBD is composed of the characterized coplanar patch antenna, a reflective PCB tag, an SMA connector, and its adapter for connecting the antenna and tag. The reflective PCB tag shown in Fig. 8a is developed based on our previous work [17], yet containing only the PIN diode and the control signal bias resistor, resembling the principle of the IBD. The diode either shorts or opens the antenna terminals, offering two reflection coefficients  $\Gamma_1$  and  $\Gamma_2$ , theoretically resulting in  $\Gamma_1 = -\Gamma_2 = 1$ . The reflection coefficients of the tag are measured with the VNA, shown in Fig. 8b. A modulation factor  $M = 0.591$  is achieved with  $|\Gamma_1| = -1.79$  dB at state 1 (short) and  $|\Gamma_2| = -1.17$  dB at state 2 (open). The multi-antenna DBD is composed of the characterized  $1 \times 4$  antenna array, a four-way power splitter, the same reflective PCB tag, coaxial cables, and connectors. The power splitter is used to feed the PCB tag with the total received power from all four antenna elements, achieving array gain and directivity. The 2FSK control signal is generated from either an MCU or a function generator. Such signal is applied to all four DUTs as baseband feeding during experiments.

The measurements are performed with bistatic collocated and bistatic dislocated AmBC configurations in an anechoic chamber shown in Fig. 7a and 7b, respectively. In the bistatic collocated scheme, the ambient RF source and the RX antennas are placed close to each other with a separation of 0.125 m, and the received signal is measured at the RX for various positions of the DUT. The DUT is moved from 0.25 to 4.75 m away from the center of the source and RX with 0.25 m steps. Moreover, in the bistatic dislocated scheme, the distance between the RF source and the RX is fixed to 5.0 m, and the DUT is moved between the source and RX in a straight line with 0.25 m steps. The heights of the ambient RF source, DUT, and RX are set to 1.0 m among all measurements.

For comparing measurement results with the well-known backscatter radio propagation models [18], simulations are also implemented with the realistic parameters used by measurement configurations. The propagation model for the bistatic collocated scheme is expressed by

$$P_R = \frac{P_T G_T G_R G_{BD}^2 \lambda^4 X^2 M}{(4\pi r)^4 \Theta^2 B^2 L_{BCBC}}, \quad (3)$$

where  $P_R$  denotes the RX received backscatter signal power and  $P_T$  denotes ambient source emitted signal power.  $G_T$ ,  $G_R$ , and  $G_{BD}$  are the gains at the ambient source, RX, and BD, respectively.  $X$  denotes the polarization mismatch, and  $M$  denotes the modulation factor.  $\lambda$  is the wavelength.  $r$  is the distance between the source/RX and BD.  $\Theta$  implies the on-object gain penalty of the BD.  $B$  indicates the path-blockage loss and  $L_{BCBC}$  is the cabling loss. Moreover, the model of bistatic dislocated scheme is

$$P_R = \frac{P_T G_T G_R G_{BD}^2 \lambda^4 X_f X_b M}{(4\pi)^4 r_f^2 r_b^2 \Theta^2 B_f B_b L_{BDDBC}}, \quad (4)$$

where  $X_f$  and  $X_b$  denotes the polarization mismatch of forward link (from the emitter to BD) and backscatter link

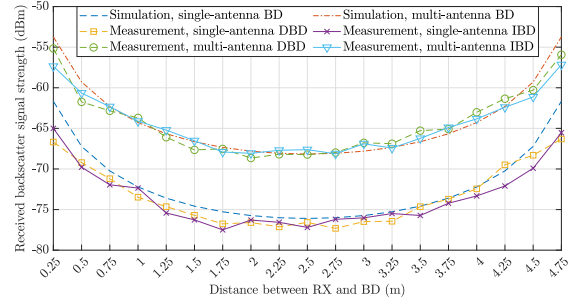
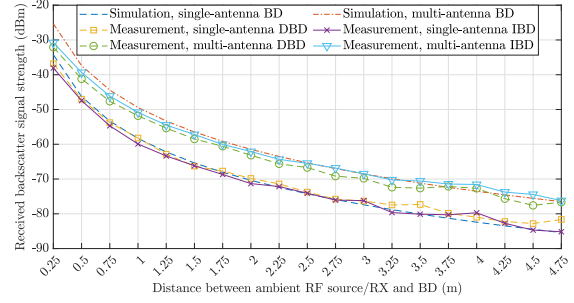


Fig. 9: OTA measurement result: (a) bistatic collocated configuration, (b) bistatic dislocated configuration.

(from the BD to RX), respectively.  $r_f$  and  $r_b$  is the distance of the forward and backscatter link, respectively.  $B_f$  and  $B_b$  is the path-blockage loss of the forward and backscatter link, respectively.  $L_{BDDBC}$  is the cabling loss.

The characterized single antenna and antenna array gains are utilized as gains  $G_{BD}$  at DUTs. The reflection coefficients  $\Gamma$  and modulation factor  $M$  of the IBDs are difficult to measure. Alternatively, such parameters of the DBD are measured and utilized in simulations as the benchmark. Antennas of the RF source, RX, and BDs are vertically polarized, therefore it is assumed that there is no polarization mismatch loss between them. Gain penalty and path-blockage loss are neglected and considered 0 dB loss for them. The measured cabling loss is 2.72 dB and 4.15 dB for the bistatic collocated and dislocated setup, respectively.

#### IV. RESULTS AND EVALUATION

In this section, measurement and simulation results shown in Fig. 9 are discussed and evaluated from two aspects: A). multi-antenna diversity gain at the BDs; B). backscattering performance of IBDs and DBDs, compared with radio propagation simulation.

##### A. Multi-antenna diversity gain

In the bistatic collocated AmBC setup, an average diversity gain of 8.75 dB at the four-antenna IBD is observed over all distances, compared with the single-antenna IBD. Similarly, such gain of 6.36 dB at the four-antenna DBD is observed compared with the single-antenna DBD. Furthermore, in the

bistatic dislocated setup, an average diversity gain of 9.01 dB at four-antenna IBD is observed over all distances, compared with the single-antenna IBD. Similarly, such gain of 8.99 dB at four-antenna DBD is observed compared with the single-antenna DBD. Such observed diversity gains indicate that the multi-antenna IBD directly improves the received signal power and hence the SNR of the backscatter signal.

### B. Performance of IBDs versus DBDs

The performance of the single- and multi-antenna IBDs regarding the RX received backscatter signal power is investigated and compared with the benchmark DBDs. The mean absolute difference of received power between the single-antenna IBD and DBD is 1.13 and 0.93 dB for the collocated and dislocated schemes, respectively. Such difference between the four-antenna IBD and DBD is 1.42 and 0.75 dB, respectively. Therefore, both IBDs and DBDs demonstrate equivalent performance. However, the IBDs offer the benefits of more compact design, lower cost, and greater flexibility.

Furthermore, the backscatter radio propagation models [18] are simulated for the two AmBC schemes. The root mean square error (RMSE) between model-predicted and measured backscatter signal strength at the RX is utilized for evaluating the measurement results of the IBDs. In the bistatic collocated scenario, the RMSE is 1.35 and 1.61 dB for the single- and four-antenna IBD, respectively. In the bistatic dislocated scenario, the RMSE is 1.81 and 1.32 dB for the single- and four-antenna IBD, respectively. Such results validate that the performance of fabricated IBDs is in agreement with the model prediction using realistic parameters of measurement setups.

## V. CONCLUSION

In this paper, we design and fabricate flexible inkjet-printed single- and multi-antenna integrated backscatter devices for indoor backscatter radios at the 2.4 GHz ISM band. We validate the prototypes with received backscatter signal power measurements. The four-antenna IBD brings approximately 9 dB diversity gain compared with the single-antenna IBD, which can directly improve the received backscatter signal strength and hence its SNR. We notice that the performance of the IBDs and DBDs are at the same level, yet the IBDs take significant advantage of low-cost and low-complexity virtues. We also validate fabricated IBDs performance that matches the model prediction using realistic parameters of measurement setups. The results indicate that our IBDs are good candidates for enabling green AmBC and ambient IoT in future communication systems. Our work on beamforming and multiple-input and multiple-output (MIMO) capability of the IBD is ongoing for the next publication.

## ACKNOWLEDGMENT

The authors appreciate Matti Vaaja, Jari Holopainen, Aleksandr Kuznetsov, and Kalle Koskinen for discussions. The authors also acknowledge the funding through Academy of Finland BESIMAL (Decision No. 334197), WALLPAPER (Decision No. 352912), and Aalto University, Department of Information and Communications Engineering.

## REFERENCES

- [1] 3GPP, "Study on ambient IoT (Internet of Things) in RAN," 3rd Generation Partnership Project (3GPP), Technical Specification TS 38.848, Jun. 2023, version 0.2.0.
- [2] J. Liao, X. Wang, K. Ruttik, R. Jäntti, and D.-T. Phan-Huy, "In-band ambient FSK backscatter communications leveraging LTE cell-specific reference signals," *IEEE Journal of Radio Frequency Identification*, vol. 7, pp. 267–277, 2023.
- [3] V. Liu, A. Parks, V. Talla, S. Gollakota, D. Wetherall, and J. R. Smith, "Ambient backscatter: Wireless communication out of thin air," *ACM SIGCOMM CCR*, vol. 43, no. 4, pp. 39–50, 2013.
- [4] R. Duan, X. Wang, H. Yiğitler, M. U. Sheikh, R. Jäntti, and Z. Han, "Ambient backscatter communications for future ultra-low-power machine type communications: Challenges, solutions, opportunities, and future research trends," *IEEE Communications Magazine*, vol. 58, no. 2, pp. 42–47, 2020.
- [5] M. U. Sheikh, B. Xie, K. Ruttik, H. Yiğitler, R. Jäntti, and J. Hämäläinen, "Ultra-low-power wide range backscatter communication using cellular generated carrier," *Sensors*, vol. 21, no. 8, 2021.
- [6] Y.-C. Liang, Q. Zhang, J. Wang, R. Long, H. Zhou, and G. Yang, "Backscatter communication assisted by reconfigurable intelligent surfaces," *Proceedings of the IEEE*, vol. 110, no. 9, pp. 1339–1357, 2022.
- [7] X. Wang, H. Yiğitler, and R. Jäntti, "Gaining from multiple ambient sources: Signaling matrix for multi-antenna backscatter devices," *IEEE Wireless Communications Letters*, vol. 12, no. 3, pp. 491–495, 2023.
- [8] X. Wang, H. Yiğitler, R. Duan, E. Y. Menta, and R. Jäntti, "Coherent multiantenna receiver for BPSK-modulated ambient backscatter tags," *IEEE Internet of Things Journal*, vol. 9, no. 2, pp. 1197–1211, 2022.
- [9] C. Chen, G. Wang, H. Guan, Y.-C. Liang, and C. Tellambura, "Transceiver design and signal detection in backscatter communication systems with multiple-antenna tags," *IEEE Transactions on Wireless Communications*, vol. 19, no. 5, pp. 3273–3288, 2020.
- [10] C.-H. Kang, W.-S. Lee, Y.-H. You, and H.-K. Song, "Signal detection scheme in ambient backscatter system with multiple antennas," *IEEE Access*, vol. 5, pp. 14 543–14 547, 2017.
- [11] A. M. Hayajneh, H. Al-Obiedollah, H. B. Salameh, M. Merenda, S. M. Hayajneh, S. A. R. Zaidi, and D. C. McLernon, "Performance analysis of drone assisted multiple antenna backscatter IoT sensor network," in *2021 8th IOTSMS*, 2021, pp. 1–7.
- [12] H. Guo, Q. Zhang, S. Xiao, and Y.-C. Liang, "Exploiting multiple antennas for cognitive ambient backscatter communication," *IEEE Internet of Things Journal*, vol. 6, no. 1, pp. 765–775, 2019.
- [13] J. Wiklund, A. Karakoç, T. Palko, H. Yiğitler, K. Ruttik, R. Jäntti, and J. Paltakari, "A review on printed electronics: Fabrication methods, inks, substrates, applications and environmental impacts," *Journal of Manufacturing and Materials Processing*, vol. 5, no. 3, 2021.
- [14] B. S. Cook, B. Tehrani, J. R. Cooper, and M. M. Tentzeris, "Multilayer inkjet printing of millimeter-wave proximity-fed patch arrays on flexible substrates," *IEEE Antennas and Wireless Propagation Letters*, vol. 12, pp. 1351–1354, 2013.
- [15] J. Kerminen, B. Xie, L. Mela, A. Karakoç, K. Ruttik, and R. Jäntti, "Low-cost thin film patch antennas and antenna arrays with various background wall materials for indoor wireless communications," *Flexible and Printed Electronics*, vol. 8, no. 2, p. 025013, may 2023.
- [16] J. Kimionis, A. Georgiadis, S. N. Daskalakis, and M. M. Tentzeris, "A printed millimetre-wave modulator and antenna array for backscatter communications at gigabit data rates," *Nature Electronics*, vol. 4, no. 6, pp. 439–446, 2021.
- [17] B. Badihi, A. Liljemark, M. U. Sheikh, J. Lietzén, and R. Jäntti, "Link budget validation for backscatter-radio system in sub-1GHz," in *2019 IEEE WCNC*, 2019, pp. 1–6.
- [18] J. D. Griffin and G. D. Durgin, "Complete link budgets for backscatter-radio and RFID systems," *IEEE Antennas and Propagation Magazine*, vol. 51, no. 2, pp. 11–25, 2009.
- [19] "Silver nano list of products," accessed: 04-08-2023. [Online]. Available: <https://www.mpm.co.jp/electronic/eng/silver-nano/line-up.html>
- [20] "SMP1345 series: Very low capacitance plastic packaged silicon PIN diodes," accessed: 04-08-2023. [Online]. Available: <https://www.skyworksinc.com/Products/Diodes/SMP1345-Series>
- [21] "StarLab: Multi-probe systems," accessed: 04-08-2023. [Online]. Available: <https://www.mvg-world.com/en/products/antenna-measurement/multi-probe-systems/starlab>